ELSEVIER

Bone Vol. 16, No. 5
May 1995:533–544

The Strength of a Calcified Tissue Depends in Part on the Molecular Structure and Organization of its Constituent Mineral Crystals in their Organic Matrix

W. J. LANDIS

Department of Orthopedic Surgery, Harvard Medical School and the Children's Hospital, Boston, MA 02115, USA

High-voltage electron-microscopic tomographic (3D) studies of the ultrastructural interaction between mineral and organic matrix in a variety of calcified tissues reveal different crystal structural and organizational features in association with their respective organic matrices. In brittle or weak pathologic or ectopic calcifications, including examples of osteogenesis imperfecta, calciphylaxis, calcergy, and dermatomyositis, hydroxyapatite crystals occur in various sizes and shapes and are oriented and aligned with respect to collagen in a manner which is distinct from that found in normal calcified tissues. A model of collagen–mineral interaction is proposed which may account for the observed crystal structures and organization. The results indicate that the ultimate strength, support, and other mechanical properties provided by a calcified tissue are dependent in part upon the molecular structure and arrangement of its constituent mineral crystals within their organic matrix. (*Bone 16:533–544; 1995*)

Key Words: Mineralization; Mineral strength; Mineral; Collagen; Osteogenesis Imperfecta; Calcergy; Calciphylaxis; Dermatomyositis; High-voltage electron microscopy; Electron-microscopic tomography; 3D reconstruction.

Introduction

The biological process of mineralization among vertebrates involves a complex series of events which culminates in the deposition of the calcium phosphate salt, hydroxyapatite, in a principally proteinaceous, organic matrix composed predominantly of collagen in all tissues except enamel, otoliths, and a few other exceptions. Together, hydroxyapatite and collagen interact to form a composite material whose mechanical, physical–chemical, and biological properties differ considerably from those of either constituent separately. Thus, the nature and character of the mineral and collagenous matrix, as well as the mineral–matrix association, are critical for the strength of a calcified tissue such as bone. From a material point of view, the strength of any tissue derives principally from two sources, its elastic (or stiffness) and plastic components. For a calcified tissue, elasticity is related to the mineral phase of the tissue and plasticity to the matrix.[5,12,25] Precisely how these two material properties are affected by the mineral and matrix or their interplay is not fully understood.

The study reported here has examined aspects of the structural features of mineral and matrix in a number of unusual calcifications characterized by their brittleness and weakness. These have included examples of osteogenesis imperfecta, calciphylaxis, calcergy, and dermatomyositis in which the constituent mineral crystal sizes and shapes and the crystal location, orientation, and alignment with respect to collagen have been determined by high-voltage electron-microscopic tomography.[17] This novel method provides ultrastructural images of the features of interest in three dimensions (3D) and yields microscopic information which cannot readily be obtained from conventional two dimensional electron micrographs.[32] The tomographic results shown in this work indicate that the parameters analyzed are distinct in the pathological and ectopic calcifications compared to normal calcified tissues. A model of collagen–mineral interaction is presented which may explain the structure and organization of the observed calcified deposits. The data are interpreted to suggest a possible fundamental relation between the strength of a calcified tissue and its mineral and matrix constituents.

Materials and Methods

This work involved the study of brittle and weak tissue from four examples of abnormally calcified vertebrate material. While these may be distinct with respect to collagen and noncollagenous protein composition, among other differences for instance, the general pattern of calcification reported below is similar in these cases. Each tissue is described separately below.

Osteogenesis imperfecta (brittle bone disease[6]): The mineralizing Achilles tendons[30] were examined from a mouse mutant which produces α1(I) collagen homotrimer and replicates a moderate to severe form of osteogenesis imperfecta.[9] The mutant studied was homozygous recessive for the oi character (*oim/oim*) and the leg tendons and other portions of the skeleton of the animals, 110–463 days old, were calcified but brittle. Tissue was kindly provided by Drs. S. D. Chipman, D. J. McBride, and J. R. Shapiro (Division of Geriatric Medicine, Johns Hopkins University School of Medicine).

Calciphylaxis: Calciphylaxis is a pathologic soft tissue calcification which may be induced experimentally.[3,36] The specimens examined in this study were obtained from the skin of white female Sprague-Dawley rats weighing about 100 g each. Tissue was provided by Dr. George Boivin (INSERM Unite 234, Faculte Alexis Carrel, Lyon, France), and topical calciphylaxis was induced following the procedures of Boivin[2] and Tochon-

Address for correspondence and reprints: Dr. William J. Landis, Enders Building—Room 284, Children's Hospital, 300 Longwood Avenue, Boston, MA 02115, USA.

8756-3282/95/$9.50
8756-3282(95)00076-P

Bone Vol. 16, No. 5
May 1995:533–544

Danguy et al.[47] Animals were sensitized by gastric intubation of 1 mg dihydrotachysterol (AT 10, Bayer, Germany) per 100 g body weight. After 24 h, each animal was given a subcutaneous injection of ferrous chloride ($FeCl_2 \cdot 4H_2O$) at a dose of 50 μg per 100 g body weight. Injection was given in the medial, posterior region of the back of the animals. While rats were anesthetized with ether or Nembutol, subcutaneous calcified tissue was obtained at intervals between 18 h and 30 days following injection.

Calcergy: A second example of a pathologic soft tissue calcification, calcergy was experimentally induced in rat skin in the same manner as that described for calciphylaxis, except that 100 μg of potassium permanganate ($KMnO_4$) in aqueous solution per 100 g animal body weight was used for injection.[3,13,55] Skin samples were provided by Dr. G. Boivin and were obtained at intervals between 36 h and 22 days after injection.

Dermatomyositis: The pathologic calcification[4] was obtained on biopsy from human (adult female) skin. The soft tissue plaque observed grossly was a firm, dense mass.

The various calcified specimens were each treated similarly for microscopic examination. After dissection, small (~1 mm^3) pieces of the tissues were treated with either 2.5% glutaraldehyde and 1% osmium tetroxide or 100% ethylene glycol and Cellosolve, dehydrated in graded ethanols, and embedded in Epon resin. Details of these aqueous and anhydrous procedures are given elsewhere.[31] Toluidine blue–stained 1-μm sections were cut from Epon-embedded blocks to determine morphological features of the tissues; and uranyl acetate– and lead citrate–stained 80-nm sections were obtained by ultramicrotomy from the regions of mineral deposition, documented by photography in a JEOL 100C or Philips EM 300 transmission electron microscope operated at 60–100 kV with a liquid nitrogen cold trap to reduce contamination artifacts.

The same tissue-block regions photographed by conventional electron microscopy were next cut into 0.25- or 0.5-μm sections, some of which were stained with uranyl and lead salts. These were viewed and photographed at 1.0 MV in the Albany (NY) AEI-EM7 high-voltage electron microscope, equipped and operated with a liquid nitrogen cold trap. The areas of each of the respective specimen sections containing early mineral deposits were recorded at 10,000× or 12,500× magnification in a 2° tilt series over a ±50°–60° range. Each micrograph was digitized using an EICONIX EC 78/99 digital camera with a pixel size of 1.3 or 3.2 nm. Digitized images were rotationally and translationally aligned as described previously.[33,37] Images were also normalized for density differences and reconstructed by weighted back-projection.[18,38] All 3D reconstructions were low-pass filtered to their limiting resolution of ~6 nm[10,41] and viewed as single slices, shaded surfaces,[42] or rendered volumes.[35] SPIDER (Wadsworth Center for Laboratories and Research, Albany, NY) or Voxel-View (Vital Images, Inc., Fairfield, IA) software was utilized for image processing, which displayed continuous rotations of the reconstructions through a wide range of tilt angles. Additional details of these methods are presented in McEwen et al.[39] and Landis et al.[32]

Selected area electron diffraction of unstained thick sections of certain of the tissues was performed at 1.0 MV with liquid nitrogen cooling. A 100-μm diffraction aperture was used and the microscope camera length was 2.0 m. The circular diffraction zone was ~3.5 μm in diameter at the specimen plane.

Results

Figure 1 presents the typical ultrastructure of the mineralizing tendon matrix from a 110-day-old *oim/oim* mouse mutant. At this level of examination, the extracellular architecture of the tendon is dominated by the presence of collagen fibrils generally arranged parallel to each other. There are also many small vesicles located in narrow spaces between the fibrils. At an increasing magnification, early mineral deposits appear as electron densities of various sizes and shapes, disposed in a scattered fashion among the numerous collagen fibrils **(Figure 2).** In this micrograph, the section is not stained and collagen and other organic matrix constituents are only faintly visible. In some locations, the mineral exhibits a periodicity corresponding to the characteristic collagen banding pattern. Extensions or spikes of mineral occur in some instances along the periphery of a number of dense deposits. Such spikes may follow the long axis direction of individual collagen fibrils but frequently they are observed in other orientations. Representative electron diffraction patterns taken under high voltage are variable and show both generally random crystal orientation (Figure 2, upper inset) and a suggestion of some orientation including that in which crystal *c*-axes are aligned along the collagen long axis (Figure 2, lower inset). **Figure 3** shows a stereoscopic pair of images taken from the 3D reconstruction of three extensions originating at the surface of a larger mineral aggregate illustrated in Figure 2. The composite crystals of the extensions are irregular in size and shape and are apparently longer than wider with dimensions on the order of 400 × 125 × 60 nm. The crystals also appear to be block-like and any discrete, smaller and thinner composite platelets are difficult to distinguish. The crystals have their longest dimension aligned with the collagen long axis at this location, but other crystals, such as that shown in **Figure 4,** have no definite alignment with respect to the collagen long-axis direction.

The structural appearance of the mineral deposited in calciphylaxis of rat skin **(Figure 5)** is different from that observed in the *oim/oim* mouse. The subcutaneous tissue is marked by loose arrangements of collagen fibrils disposed in different directions. In the apparent beginning stages of calcification, noted by smaller sites of limited electron density, the mineral seems to be incorporated entirely into individual fibrils, and there is little evidence for extrafibrillar mineral in the affected areas. Sites of heavier density, presumably representing increasing calcification, have long, extended, generally cylindrical shapes following the contours of the fibrils. Notably, these densities are of variable width or diameter, considerably greater than the diameters of the fibrils themselves. The deposits are characteristically tapered at the transition zone between unmineralized and mineralized portions of the fibrils. The movie and stereoscopic images obtained from 3D reconstruction of the tapered ends of mineral **(Figure 6)** show a strict association of crystals within the cylindrical confines of collagen. The crystals in this instance are apparently fused together into rather large, long, solid-looking rod-like structures which narrow into the unmineralized fibril. There is neither the periodic location of the crystals within collagen nor the presence of any ordered deposition of mineral following the collagen hole and overlap zones as observed in normal collagen calcification.

Typical structural features of calcergy are shown in **Figure 7.** The extracellular tissue matrix contains numerous, relatively widely separated collagen fibrils formed into many discrete bundles. Within any particular bundle in the sensitized areas of the rat skin, nearly every fibril is mineralized. As also found in calciphylaxis, the calcification appears exclusively within the fibrils at the outset of mineral deposition. Progressive calcification is noted by increasing electron density extending farther along the lengths of the fibrils and wider than their diameters. The mineral again appears to narrow at the transitional zone between uncalcified and calcified portions of fibrils. Stereoscopic images from 3D reconstructions of newly forming mineral in

Figure 1. Photomicrograph of a thin (80-nm) section of the mineralizing tendon from a 110-day-old *oim/oim* mouse mutant, examined by conventional (80 kV) electron microscopy. The tissue has been fixed with glutaraldehyde and osmium tetroxide and stained with uranyl and lead salts. Matrix ultrastructure shows a few large tendonoblasts involved in the synthesis and secretion of extracellular constituents, principally including collagen fibrils [α1(I) homotrimers in this case] (C), which are assembled in parallel fashion to one another and to the tendon long axis (heavy arrow). Some small vesicles (V) appear between fibrils. At this level of structure and organization, the general appearance of this model for osteogenesis imperfecta is similar to normal tendon. Mineralization has not occurred in the tendon region illustrated. Original magnification ×5,250. Bar = 5.0 μm.

calcergy **(Figure 8)** resemble those obtained in calciphylaxis. The early crystals lie within the fibrils and are shaped like long, solid rods tapered at their extremes. Fusion of closely associated rods would appear to produce thicker mineral deposits. Periodic deposition of crystals corresponding to collagen hole and overlap zones cannot be distinguished.

Dermatomyositis is marked by numerous collagen fibrils disposed in an apparently disordered manner within extracellular tissue matrices **(Figure 9).** In this pathology, the early crystals on image reconstruction **(Figure 10)** appear as relatively small deposits confined once more within individual fibrils. The general crystal shape resembles a short, thin spear and the crystals, themselves, lie in many different directions. In the initial stages of the calcification in this example, there is little evidence of association of crystals with each other.

Discussion

One of the major functions of the vertebrate skeleton is to provide mechanical strength for support and protection of tissues and organs. Characteristic features of skeletal mechanical strength and the adaptive nature of the skeleton in terms of its architectural accommodation of natural or applied forces have been described in some detail (see, for example, Burstein et al.,[5] Carter,[7] Curry,[11,12] Einhorn,[14] Frost,[19–22] and Jee et al.[24]), but the precise underlying biomechanical and biological basis for skeletal strength remains poorly understood. In general, the inherent strength and other mechanical properties of the skeletal system are thought to depend on an interaction between its inorganic and organic matrix constituents.[5,12] This concept is supported, for example, by the observation that the composite formed between the normal mineral salt, hydroxyapatite, and collagen, the principal organic component of the vertebrate skeleton, is able to resist a wide range of compressive or tensile forces whereas either material alone cannot.

On the other hand, the relationship between strength and mineral–organic matrix interaction is more complicated than one simply requiring the presence of a hydroxyapatite–collagen composite: Certain cases of pathologic mineralization such as osteogenesis imperfecta, comprised of hydroxyapatite–collagen, yield characteristically brittle material. The present study of this and other instances of a varied mineralization attendant with a quality

Bone Vol. 16, No. 5
May 1995:533–544

Figure 2. Early mineralization of the tendon matrix in a 110-day-old *oim/oim* mouse mutant. This unstained thick (0.25 μm) section observed by high-voltage microscopy was treated by anhydrous means with ethylene glycol and electron-dense mineral deposits (M) are the principal structural features which are conspicuous. Collagen (C) is associated with the mineral in this area and its periodicity is sometimes enhanced by the crystals (arrows). Deposits of various sizes and electron densities appear rather randomly in the matrix and, along the peripheries of some relatively larger deposits, unusual spikes of mineral may occur (arrowheads), following the long axis direction of the fibrils (heavy arrow). Denoted by the outlined boxes, two small volumes of the matrix-containing mineral were reconstructed to examine the composite crystals more completely in 3D. Two insets show different selected area electron diffraction patterns typical of the mineral in unstained thick sections of the *oim/oim* mutant (but not the field shown in Figure 2, which has insufficient mass to generate a coherent pattern). The reflections of both inset patterns are characteristic of a poor crystalline hydroxyapatite. The upper inset with nearly complete reflections and no evidence of arcing represents crystals generally randomly oriented. The lower inset has faint, narrow arcs corresponding to the apatite 211, 112, and 300 reflections (single arrowheads) and also to the 002 and 004 (double arrowheads) reflections. The latter indicate some crystal *c*-axes are oriented along the collagen long axis. Similar patterns are obtained in high-voltage microscopy from the other examples of mineralized tissues reported here. Magnification ×30,300. Bar = 1.0 μm.

of abnormal material strength provides insight into the possibility that skeletal mechanical properties are dependent, at least in part, upon the molecular structure and arrangement of the respective constituent mineral crystals within their organic matrix.

This report has investigated the ultrastructural relation between the early mineral crystals and the organic matrix serving as the framework for their deposition in four cases of abnormal, brittle calcification, including osteogenesis imperfecta. In all four examples compared to normally calcifying vertebrate tendon and bone,[1,32,39] the crystals are found to be unusual in two principal aspects, their habit and their spatial relation with respect to collagen. The normally mineralizing tendon and bone characterized by high-voltage electron-microscopic tomography in the same manner as presented here contain crystals whose shapes resemble irregular, thin platelets of sizes reaching ~170 × 45 × <6 nm.[1,32] The crystals are clearly located in both the hole and overlap regions of collagen[39] and are aligned closely parallel to one another and to the long axis of the fibrils with which they associate.[1,32] In the four examples of abnormal calcification examined here, the crystals appear not as thin platelets but as relatively thick, bulky blocks or narrow spear-shaped structures whose individual sizes exceed as much as three- to ten-fold the dimensions of normal tendon and bone crystals. In addition, development of the crystals is more obvious in their length than in other dimensions, a result leading to the observed long, spikelike nature of the deposits in the abnormal tissues. In

Figure 3. Enlargement of one region outlined in Figure 2 and shown in stereoscopy. The two images were obtained from the 3D reconstruction and are separated by a 20° angular difference. The spikes or extensions of mineral are thick and block-like in appearance, irregular in size and shape, and quite distinct from thin platelets which are characteristic of the mineral crystals found in normal leg tendon calcification of avians.[32] These particular crystals of the mouse have their longest dimension aligned with the collagen long-axis direction (arrow) as would be expected in normal conditions of mineralization, but there is no clear association of the deposits with either the hole or overlap regions of the collagen fibrils as also occurs in normal situations.[32] Magnification ×45,000. Bar = 0.5 μm.

contrast, the normal tendon and bone generate approximately parallel arrays of thin, very nearly flat crystal bands or sheets.[32] With regard to their specific spatial location, the crystals in the abnormally mineralized examples are unquestionably associated with collagen, but they are not found as conspicuously following the hole and overlap regions of the fibrils as their normal counterparts. Finally, the pathologic mineralizations are different from normal in that their respective crystals are aligned only inconsistently with respect to the collagen long axes rather than strictly in parallel with them.

It is interesting to consider certain other structural details in the *oim/oim* mouse model of osteogenesis imperfecta. From the present and additional[31] microscopic 3D reconstructions of both unmineralized and mineralized portions of tendons from different affected mice, collagen assembly in parts of the tissue appears to be disorganized: Many individual fibrils are twisted and kinked, and the characteristic 64–70 nm collagen period, describing the hole and overlap regions of aggregated molecules,[23] is out of register across some adjacent fibrils. While unproved, such apparently irregular or disrupted collagen regions may be the result of the synthesis of a matrix primarily composed of α1(I) homotrimers in this model of osteogenesis imperfecta. Alternatively, or perhaps in addition, other possible alterations may exist in the *oim/oim* case which could also affect the structural integrity of the matrix. In this regard, studies in osteogenesis imperfecta of collagen synthesis and secretion,[43,44] alterations in procollagen genes,[6,28,40,45,46,48] abundance of minor collagen species or noncollagenous proteins,[15,52] differences in collagen crosslink characteristics,[53] and modifications in crystal sizes and mineral[8,16,49,51] are important to consider.

Whatever the actual underlying reasons for the changes found in the matrix of the *oim/oim* mouse, the present tomographic observations that collagen fibrils in portions of the calcifying *oim/oim* tendon are different from normal tissue in their alignment and general organization may be significant in terms of both the mineral deposited in the matrix and the strength of the tissue. With respect to the mineral, the 3D data lead to a possible explanation, given here for the first time and depicted in **Figures 11 and 12,** for the nature of the mineral crystals in not only osteogenesis imperfecta but also the other three pathologic examples studied, each containing crystals unusual in their size and shape and their location and arrangement with respect to collagen. Figure 11 illustrates the 3D assembly and mineralization of a normal collagen array based on recent tomographic studies of Landis et al.[32] and consistent with earlier work published by Katz and Li,[26] Katz et al.,[27] Traub et al.,[50] Yamauchi et al.,[57]

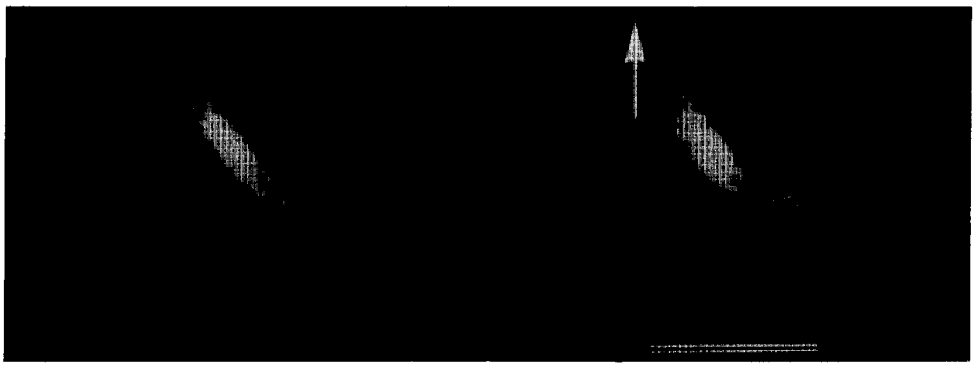

Figure 4. Mineral deposits from the second region of Figure 2 and shown as a stereoscopic pair of images (20° angular difference) taken from the 3D reconstruction. A smaller, thin deposit (arrowhead) is aligned in the same direction as the collagen fibril long axis (arrow), but the larger, more disperse-appearing deposit is not parallel to its neighbor and is oblique to the collagen long-axis direction. The size and shape of these deposits are unlike those observed in normal calcification and the crystals again have no definite association with the collagen period. Magnification ×45,000. Bar = 0.5 μm.

Bone Vol. 16, No. 5
May 1995:533–544

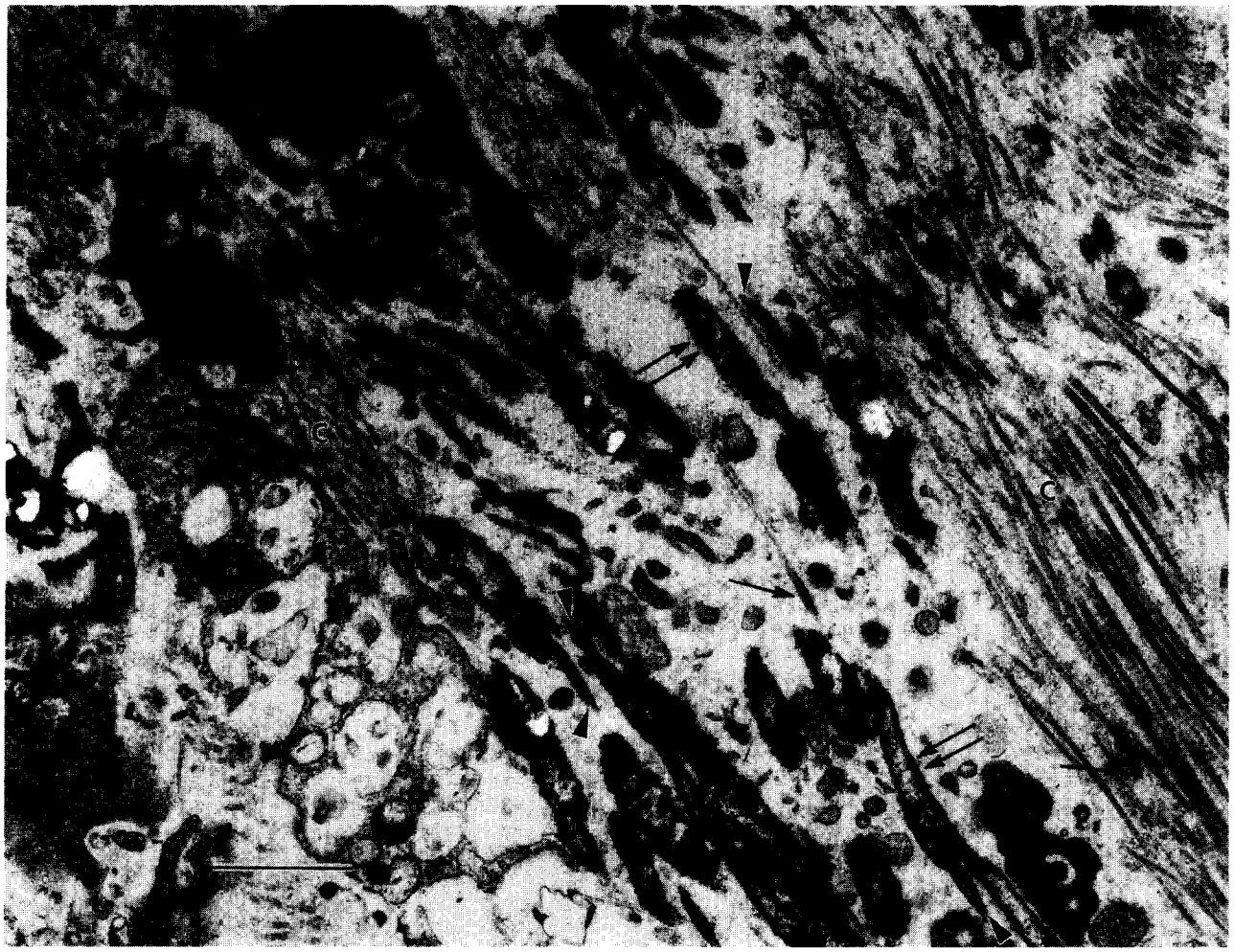

Figure 5. Stained thin section of calciphylaxis in rat skin, treated for conventional (80 kV) electron microscopy with glutaraldehyde and osmium tetroxide. The sample was obtained 30 days after ferrous chloride injection. The tissue consists of numerous, loosely arranged collagen fibrils (C) of different sizes and dispositions. Mineral is closely associated with only the fibrils, deposited entirely within them at early stages of calcification (single arrows) and then later apparently extending beyond the fibril diameters as if forming a mineral coating over the collagen surfaces (double arrows). The deposits become narrow within the fibrils at the junction between their unmineralized and mineralized regions (arrowheads). Magnification ×19,000. Bar = 1.0 μm.

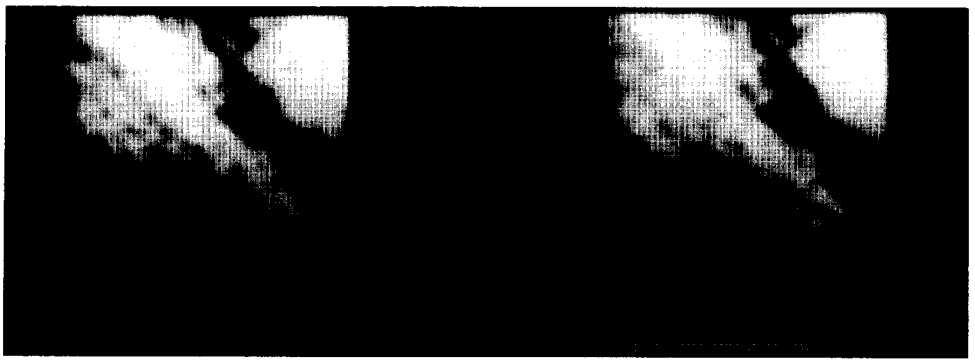

Figure 6. Stereoscopic images (20° angular difference) from the high-voltage 3D reconstruction of the tapered mineral within a collagen fibril in calciphylaxis. The fibril is one of many in an unstained thick (0.25 μm) section from the skin of a 4-week-old rat, treated with ethylene glycol. The mineral appears to be fused into relatively large, extended, rod-shaped structures, following the fibril long-axis direction. Such calcified forms are very distinct in their size and shape from any other deposits found in normal vertebrate mineralized tissues. The mineral in calciphylaxis also has a solid appearance without the normally detectable presence of smaller, thin platelets located in association with collagen hole and overlap regions. Magnification ×50,400. Bar = 0.5 μm.

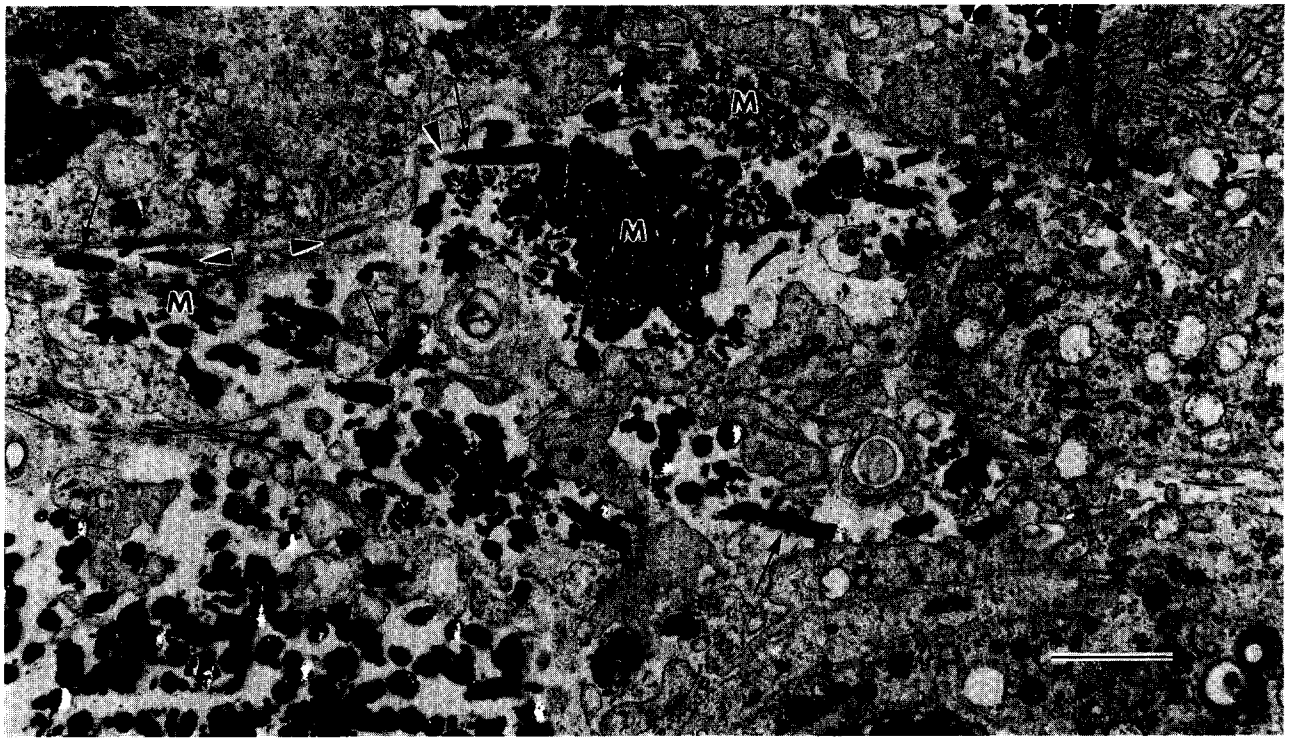

Figure 7. Calcergy in thin sections of rat skin, treated as described in Figure 5, is marked by the presence of many mineralized collagen fibrils (M) organized into bundles. The sample was obtained 22 days after injection with potassium permanganate. As with calciphylaxis, the mineralization appears to occur exclusively within the confines of the fibrils and apparently extends beyond fibril diameters as a surface coating with progressive deposition (arrows). Similar also to mineralization of collagen in calciphylaxis, the deposition in calcergy becomes tapered at locations between unmineralized and mineralized sites within the fibrils (arrowheads). Magnification ×8,100. Bar = 2.0 μm.

and Weiner and Traub[56] among others. Notable features of Figure 11 are: (1) the presence of channels or grooves in the array resulting from alignment of collagen hole and overlap zones; (2) the nucleation predominantly occurring in hole zones; (3) the development of irregularly shaped, thin crystal platelets whose growth in length follows the direction of the collagen long axes and in width follows the channels traversing the collagen arrays; and (4) the eventual formation of a series of extended, generally parallel sheets of mineral, shown more clearly in Figure 12.

This conceptual model is contrasted with that based on the tomographic observations of the pathologic mineralizations described above. Irregularities and disruptions observed in the collagenous matrix of the *oim/oim* model may be thought to occur as well in the calcified skin from calciphylaxis, calcergy, and dermatomyositis. The basis of such matrix discontinuities is proposed to be a consequence of abnormal assembly of collagen molecules whereby their hole and overlap zones are mismatched and fail to form the extensive channels or gaps characteristic of normal tissue (Figure 11). The misregistration may be such that one or a small group of hole regions in a few adjacent molecules

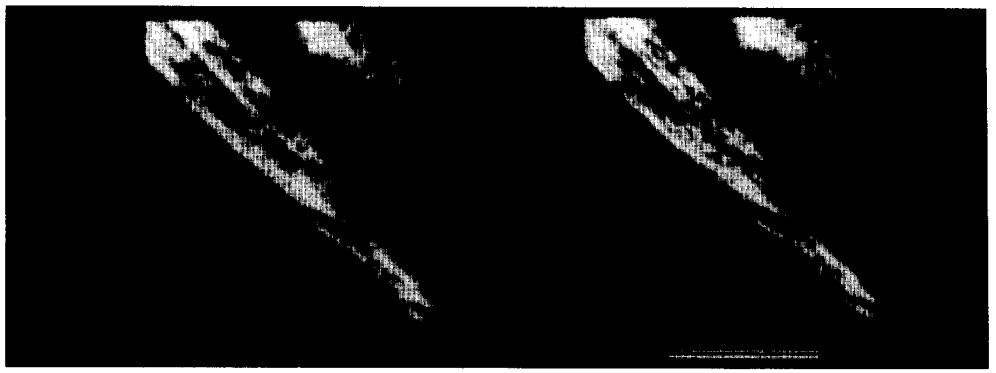

Figure 8. Mineral deposition in calcergy determined in stereoscopic images (20° angular difference) from the high-voltage 3D reconstruction of calcifying collagen fibrils. The section (0.25 μm) is unstained and was prepared by anhydrous methods with ethylene glycol. Mineral is found as solid, long rods, tapered at their ends within the collagen fibrils. Smaller, thin, platelet-shaped crystals are not detectable in the deposits of calcergy and the mineral in this abnormal calcification is not clearly located within collagen hole and overlap regions. The long axis of each of the tapered rods is generally aligned with the long axis of the associated collagen fibrils. Magnification ×40,300. Bar = 0.5 μm.

Bone Vol. 16, No. 5
May 1995:533–544

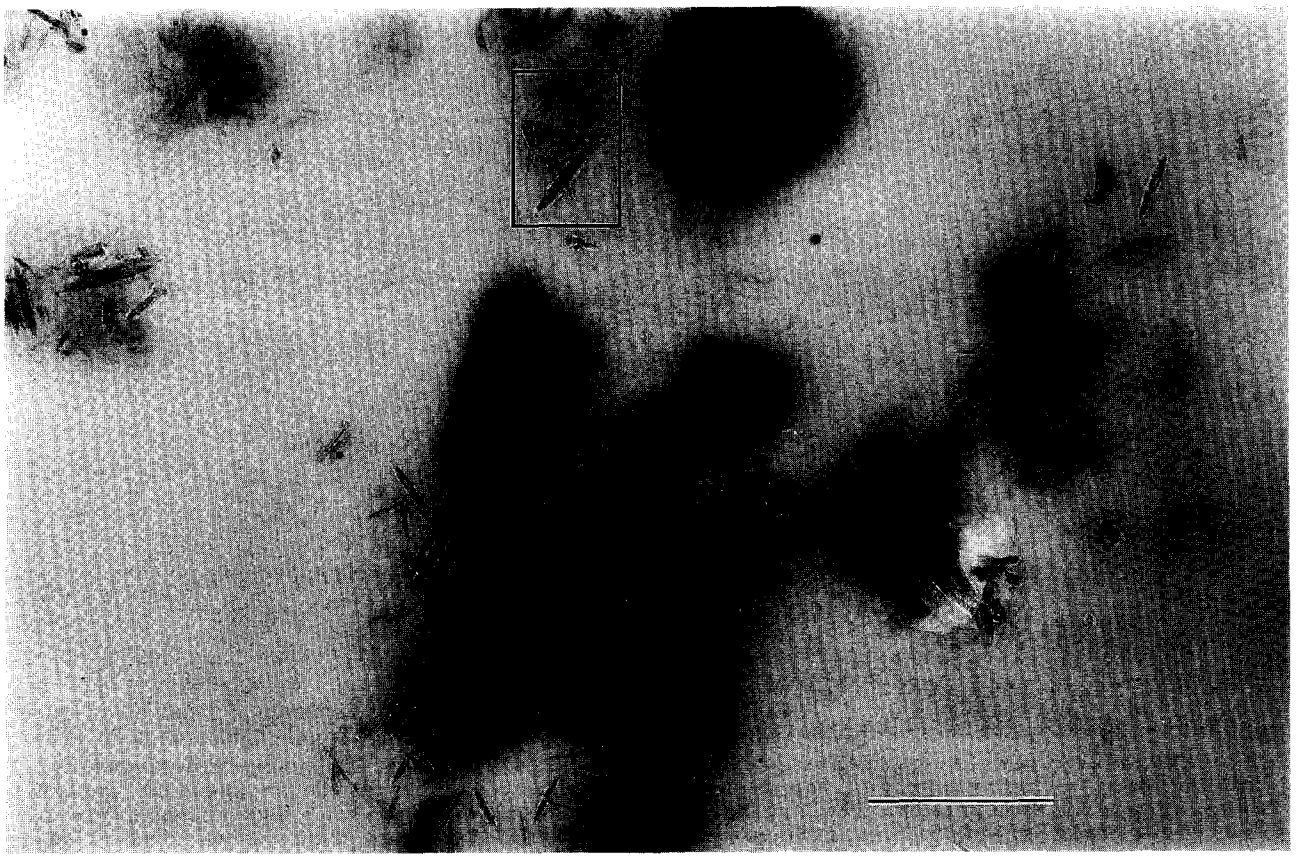

Figure 9. Photomicrograph of calcification in an unstained thick (0.25 μm) section of a human skin biopsy, prepared for high-voltage electron microscopy by anhydrous means. The deposition of mineral is associated with collagen, which is not directly visible in these preparations. Individual short, narrow deposits of mineral appear in an extremely disordered arrangement in the tissue matrix. The enclosed group of crystals was one of a number analyzed by tomography and is represented in Figure 10. A narrow halo may be observed about some crystals; its origin is unknown, perhaps the result of crystal sensitivity to electron beam exposure. Magnification ×24,300. Bar = 1.0 μm.

becomes blocked by misaligned neighbors, thereby isolating those hole zones in the molecular array. The result would lead to short, interrupted channels wherever such misregistration occurred. In addition, the matrix distortions revealed by tomography may be reflected by extended or compressed hole and overlap zones, the array sites and spaces, then, again changing from normal in these instances. Precisely what would cause the proposed poor molecular assembly of collagen is not known, but solutions may lie in studies of procollagen processing, posttranslational modifications of collagen including crosslink formation, and associations between the major type I collagen and type V molecules as well as proteoglycans.

Figure 10. A stereoscopic pair of images (20° angular difference) from the 3D reconstruction of the enclosed region of Figure 9. The mineral in dermatomyositis consists of short, thin rods whose long axes follow the long axes of associated collagen, but which have no definitive structural relation with the collagen period. Magnification ×85,300. Bar = 0.2 μm.

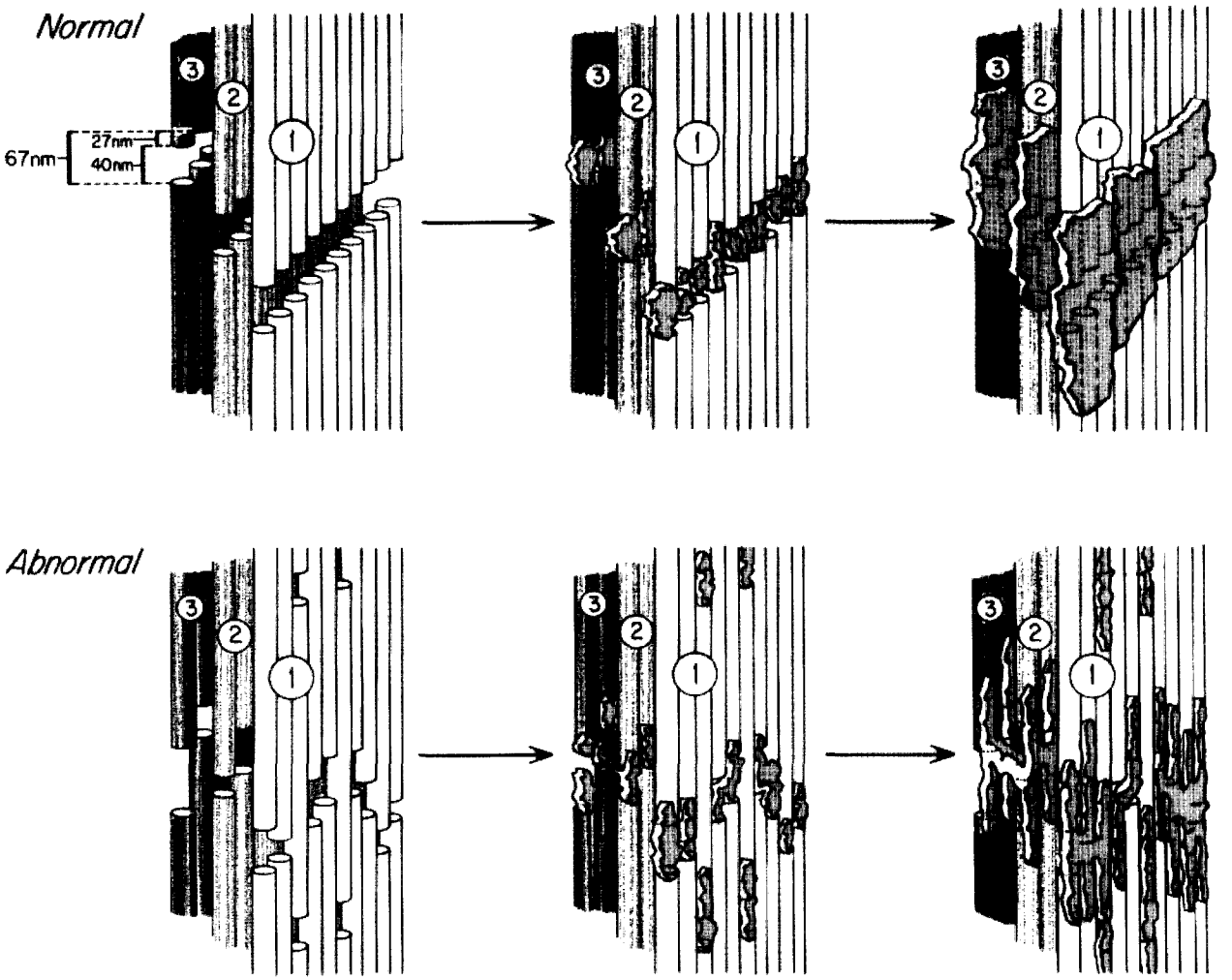

Figure 11. A schematic diagram illustrating the assembly and early mineralization of collagen molecules in a three-dimensional perspective. The upper series of drawings shows normal collagen array formation and mineral deposition as detailed elsewhere.[32] Three collagen layers are distinguished by shading and consist of a number of cylindrically shaped molecules 300 nm in length and 1.23 nm in width[34] aggregated in parallel. In the drawing, the widths of the molecules are highly exaggerated in scale compared to the lengths. The pattern of normal aggregation follows the quarter-stagger model of Hodge and Petruska[23] in which a 67-nm periodicity results from the presence of adjacent hole (40 nm) and overlap (27 nm) regions of the assembled molecules. In this instance, collagen assembly is strictly ordered and generates extensive channels or grooves[26,32,56] through the arrays, as a result of the fact that the regularity of staggering[23] creates registration of hole and overlap zones in the packing of molecules to form macromolecules and fibrils. Nucleation of mineral (upper middle drawing) occurs initially in the hole regions of the collagen arrays[39] and crystals develop preferentially in length along the collagen long axes and also in width in the spaces generated by the channels. Ultimately, broad sheets of mineral, growing principally in length and width and located parallel to each other, form in the tissue (upper right drawing).[32] The lower series of drawings depicts collagen array formation and mineralization in the pathologic examples investigated here. While the structures of these pathologic collagens are not known, it is proposed that, as a result of the absence of α2(I) chains (as in the *oim/oim* model) or changes in crosslinks, minor types of collagens, noncollagenous proteins, or other alterations (as might possibly occur in any of the abnormally mineralized cases), the assembly of collagen molecules follows a random stagger as one possibility to account for the observed changes in the crystals. In this case, the molecular array does not contain the putative extensive network of periodic channels or grooves found in normal collagenous tissues. This result is the consequence of adjacent molecules whose hole and overlap regions fail to maintain strict registration. Neighboring molecules then are misaligned and act as seals to isolate the hole zone spaces into small pockets, the spaces otherwise being uninterrupted to form the normal continuous channels (lower left drawing). Such an altered arrangement of molecules would be mimicked at the macromolecular, fibrillar, and other higher-ordered levels of collagen assembly and could lead to the unusually twisted and disorganized nature of collagen fibril matrices found in the tendons of the *oim/oim* mouse, for example. In the unusually mineralized cases, nucleation of mineral begins in hole zone regions of the array and development of the crystals still occurs preferentially in the long-axis direction of the fibrils (lower middle drawing). Since the channel spaces are limited in this assemblage, however, extensive development of crystals in width cannot be accommodated. The resultant crystals are longer than wider and eventually assume the form of narrow rods or spikes in the collagenous matrix (lower right drawing). Moreover, the misregistration of collagen may occur in adjacent layers in addition to that within a single layer. In this situation, it may be possible for hole regions to be neighboring in two or more layers of molecules, as shown by the first hole zones of layers 2 and 3 in the schematic. Such hole spaces in the depth direction of the arrays might allow thick and block-like crystals to develop (suggested by the crystals spanning the first hole zones in layers 2 and 3 in the lower middle and right drawings) as well as additional variability in crystal alignment and orientation (possibly resulting in the observed differences in electron diffraction patterns).

Bone Vol. 16, No. 5
May 1995:533–544

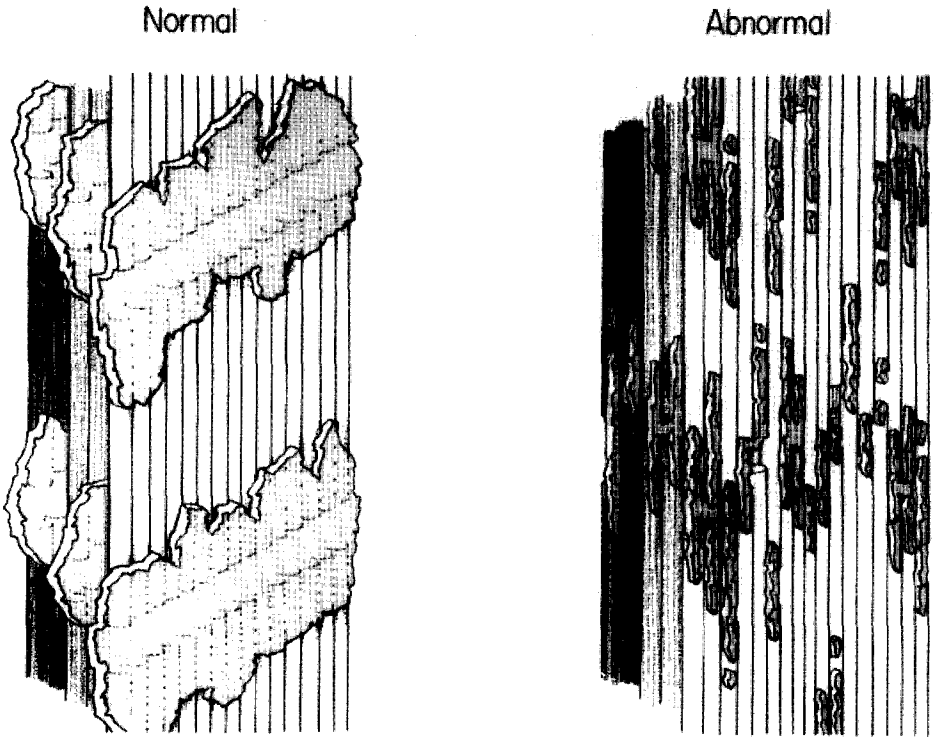

Figure 12. A schematic drawing comparing early collagen–mineral structural relations in normally calcified vertebrate tissue and the abnormal examples presented here. Normal tissue contains extended sheets of mineral, developed principally in length (along the long axes of collagen molecules) and width (along periodic channels or grooves perpendicular to the collagen long axes) and parallel to one another in neighboring collagen layers. The sheets would eventually fuse or join with one another in the same as well as adjacent collagen layers to form a thicker and broader collagen–mineral composite, producing certain mechanical properties (strength, for example) of the tissue as a result. In the pathological examples, the crystals vary in size, shape, location, alignment, and orientation in the collagen layers and as a consequence provide little continuity throughout the collagen array. This collagen–mineral composite would be weak compared to normal and could maintain only fragile integrity in terms of its mechanical properties.

In the proposed model, nucleation of mineral predominantly in collagen hole zone sites would continue as usual, as would crystal growth in length, but crystal growth in width would be retarded or prevented by the limited channel spaces within the arrays. Nucleation, but restricted growth, of crystals could occur in extended or compressed hole zones. It could also be conceived that such sites may be so altered that nucleation would be absent. Ultimately, the matrix would be composed of a combination of numerous, large and small, disconnected mineralized sites having block-like, bulky crystals in some channels accommodating them; lengthy, thin crystals following the long axis of collagen fibrils; and platelet-shaped crystal bands or sheets resembling normal structures (Figure 12). This situation, in which many deposits vary in size, shape, location, orientation, and continuity throughout the matrix, would provide the conditions for a structure with limited integrity, having only fragile mechanical support and the resulting brittle mineral which is characteristic of that found in these examples of pathological calcification.

By comparing and conceptually elaborating the 3D structural motif in the examples of normal and abnormal calcification presented here, a possible basis and fundamental relation between the strength of a calcified tissue and its mineral and matrix constituents may be suggested: *The ultimate strength, support, and other mechanical properties provided by a calcified tissue are dependent in part upon the molecular structure and arrangement of its constituent mineral crystals within their organic matrix.* Structural and organizational interactions of mineral and/or matrix constituents in addition to those at the molecular level will also contribute to the overall strength and integrity of the tissue.[14,54] For instance, it is well documented that the mineralized scaffold of cancellous bone, or the trabecular formation of cortical bone, may minimize fatigue damage and provide added load bearing and material strength to the tissue through architectural modeling at a morphological level of structure and organization.[7,20,21,25] Further investigations should generate more complete understanding as to how mineral–matrix interactions are related to their effects on mechanical properties at molecular, macromolecular, cellular, and other hierarchical levels of tissue structure and organization. At this time, the present study of 3D features in mineralization has yielded insight into molecular structure–function relationships for normal calcified tissues as well as perhaps into a possible link between genotypic and phenotypic expression in a model for osteogenesis imperfecta and, by inference, three additional examples of unusual vertebrate calcification. Extending these 3D studies to osteoporosis, osteopetrosis, Paget's disease, and other hard tissue pathologies may also give information relevant to their respective formation and possible treatment.

Acknowledgments: The author is very grateful for the help provided in many aspects of this study: in tissue preparation by Mrs. Karen J. Hodgens, Mrs. Jenny Cheung, Ms. Caryn Mello, and Mr. Mark Snowise (Children's Hospital, Boston); in high-voltage electron microscopy by Dr. Min J. Song and Ms. Diana Berkery (Wadsworth Center for Laboratories and Research, Albany); in tomography and image analysis by Mr. Rob Feuerbach, Mr. James Arena, Mr. Michael Marko, and Dr. Bruce F. McEwen (Wadsworth Center for Laboratories and Research,

Albany); in electron diffraction by Dr. William Tivol (Wadsworth Center for Laboratories and Research, Albany); in discussions of tomographic data by Dr. Joachim Frank (Wadsworth Center for Laboratories and Research, Albany); in photography by Mr. Robert Rubin (Children's Hospital, Boston); and in artwork by Ms. Pamela Battaglino. This work was supported by grants from the National Institutes of Health (AR 41452, AR 34078, and AR 34081), the National Aeronautics and Space Administration (NAG-2-538), the Peabody Foundation, and an institutional grant given by the Orthopaedic Research and Educational Foundation funded by the Bristol-Myers/Zimmer Corporation. The Wadsworth Center Biological Microscopy and Image Reconstruction Facility was supported by the National Institutes of Health and Division of Research Resources, Department of Health and Human Services/Public Health Service (Biotechnological Resource Grant RR 01219) and National Institutes of Health Grants GM 40165 and HD 22400.

References

1. Arena, J., McEwen, B. F., Song, M. J., and Landis, W. J. A study of the mineralization of bone by high voltage electron microscopic tomography. Bailey, G. W., Bentley, J., and Small, J. A., eds. Proceedings of the 50th Annual Meeting of the Electron Microscopy Society of America. San Francisco, CA: San Francisco Press; 1992; 582–583.
2. Boivin, G. Etudes chez le rat d'une calcinose cutanee induite par calciphylaxie locale. I. Aspects ultrastructuraux. Arch Anat Microsc Morphol Exp 64:183–205; 1975.
3. Boivin, G., Walzer, C., and Baud, C. A. Ultrastructural study of the long-term development of two experimental cutaneous calcinoses (topical calciphylaxis and topical calcergy) in the rat. Cell Tissue Res 247:525–532; 1987.
4. Brooke, M. H. A clinician's view of neuromuscular diseases (2nd ed.). Baltimore, MD: Williams & Wilkins; 1986.
5. Burstein, A. H., Zika, J. C., Heiple, K. G., and Klein, L. Contribution of collagen and mineral to the elastic–plastic properties of bone. J Bone Joint Surg 57A:956–961; 1977.
6. Byers, P. H. Brittle bones—fragile molecules: Disorders of the collagen gene structure and expression. Trends Genet 6:293–300; 1990.
7. Carter, D. R. Mechanical loading histories and cortical bone remodeling. Calcif Tissue Int 36:S19–24; 1984.
8. Casella, J. P. and Ali, S. Y. Abnormal collagen and mineral formation in osteogenesis imperfecta. Bone Min 17:123–128; 1992.
9. Chipman, S. D., Sweet, H. O., McBride, D. J. Jr., Davisson, M. T., Marks, S. C. Jr., Shuldiner, A. R., Wenstrup, R. J., Rowe, D. W., and Shapiro, J. R. Defective proα2(I) collagen synthesis in a new recessive mutation in mice: A model of human osteogenesis imperfecta. Proc Natl Acad Sci USA 90:1701–1705; 1993.
10. Crowther, R. A., DeRosier, D. J., and Klug, A. The reconstruction of a three-dimensional structure from projections and its application to electron microscopy. Proc R Soc London A 317:319–340; 1970.
11. Curry, J. D. The mechanical adaptations of bones. Princeton, NJ: Princeton University Press; 1984.
12. Curry, J. D. Strain dependence of the mechanical properties of reindeer antler and the cumulative damage model of bone fracture. J Biomech 22:469–476; 1989.
13. Doyle, D. V., Dunn, C. J., and Willoughby, D. A. Potassium permanganate induced calcergy: A model to study the effects of drugs on hydroxyapatite crystal deposition. J Pathol 128:63–69; 1979.
14. Einhorn, T. A. Bone strength: The bottom line. Calcif Tissue Int 51:333–339; 1992.
15. Fedarko, N. S., Mörike, M., Brenner, R., Gehron Robey, P., and Vetter, U. Extracellular matrix formation by osteoblasts from patients with osteogenesis imperfecta. J Bone Min Res 7:921–930; 1992.
16. Fischer, L. W., Eanes, E. D., Denholm, L. J., Heywood, B. R., and Termine, J. D. Two bovine models of osteogenesis imperfecta exhibit decreased apatite crystal size. Calcif Tissue Int 40:282–285; 1987.
17. Frank, J. Electron tomography: Three-dimensional imaging with the transmission electron microscope. New York: Plenum Press; 1992.
18. Frank, J., McEwen, B. F., Radermacher, M., Turner, J. N., and Rieder, C. L. Three-dimensional tomographic reconstruction in high voltage electron microscopy. J Electron Microsc Tech 6:193–205; 1987.
19. Frost, H. M. Vital biomechanics. Proposed general concepts for skeletal adaptations to mechanical usage. Calcif Tissue Int 42:145–155; 1988.
20. Frost, H. M. Intermediary organization of the skeleton. Boca Raton, FL: CRC Press; 1986.
21. Frost, H. M. Some ABC's of skeletal pathophysiology. 5. Microdamage physiology. Calcif Tissue Int 49:229–231; 1991.
22. Frost, H. M. Suggested fundamental concepts in skeletal physiology. Calcif Tissue Int 52:1–4; 1993.
23. Hodge, A. J. and Petruska, J. A. Recent studies with the electron microscope on ordered aggregates of the tropocollagen macromolecule. Ramachandran, G. N., ed. Aspects of protein structure. New York: Academic Press; 1963; 289–300.
24. Jee, W. S. S., Li, X. J., and Ke, H. Z. The skeletal adaptation to mechanical usage in the rat. Cells Mater 1:131–142; 1991.
25. Jepsen, K. J., Mansoura, M. K., Kuhn, J. L., Wu, H., Jaenisch, R., Bonadio, J. F., and Goldstein, S. A. An in vivo assessment of the contribution of type I collagen to the mechanical properties of cortical bone. Trans Orthop Res Soc 17:93; 1992.
26. Katz, E. P. and Li, S. -T. The intermolecular space of reconstituted collagen fibrils. J Mol Biol 73:351–369; 1973.
27. Katz, E. P., Wachtel, E., Yamauchi, M., and Mechanic, G. L. The structure of mineralized collagen fibrils. Connect Tissue Res 21:149–158; 1989.
28. Khillan, J. S., Olsen, A. S., Kontusaari, S., Sokolov, B., and Prockop, D. J. Transgenic mice that express a mini-gene version of the human gene for type I procollagen (COL1A1) develop a phenotype resembling a lethal form of osteogenesis imperfecta. J Biol Chem 266:23373–23379; 1991.
29. Landis, W. J. Tomographic imaging of collagen–mineral interaction: Implications for osteogenesis imperfecta. Connect Tissue Res (in press).
30. Landis, W. J., Mello, C., Snowise, M., Hodgens, K., Chipman, S., Shapiro, J., Feuerbach, R. J., Arena, J., Berkery, D., and McEwen, B. Spatial relations between vesicles and collagen in calcifying tendon from the oim/oim mouse: Three dimensional analysis by high voltage electron microscopic tomography and graphic image reconstruction. Trans Orthop Res Soc 18:671; 1993.
31. Landis, W. J., Paine, M. C., and Glimcher, M. J. Electron microscopic observations of bone tissue prepared anhydrously in organic solvents. J Ultrastruct Res 59:1–30; 1977.
32. Landis, W. J., Song, M. J., Leith, A., McEwen, L., and McEwen, B. F. Mineral and organic matrix interaction in normally calcifying tendon visualized in three dimensions by high-voltage electron microscopic tomography and graphic image reconstruction. J Struct Biol 110:39–54; 1993.
33. Lawrence, M. C. Least-squares method of alignment using markers. Frank, J., ed. Electron tomography. New York: Plenum Press; 1992; 197–204.
34. Lees, S. Considerations regarding the structure of the mammalian mineralized osteoid from viewpoint of the generalized packing model. Connect Tissue Res 16:281–303; 1987.
35. Leith, A. Computer visualization of volume data in electron tomography. Frank, J., ed. Electron tomography. New York: Plenum Press; 1992; 215–236.
36. Lian, J. B., Boivin, G., Patterson-Allen, P., Grynpas, M., and Walzer, C. Calcergy and calciphylaxis: Timed appearance of γ-carboxyglutamic acid and osteocalcin in mineral deposits. Calcif Tissue Int 35:555–561; 1983.
37. Luther, P. K., Lawrence, M. C., and Crowther, R. A. A method for monitoring the collapse of plastic sections as a function of electron dose. Ultramicroscopy 24:7–18; 1988.
38. McEwen, B. F., Radermacher, M., Rieder, C. L., and Frank, J. Tomographic three-dimensional reconstruction of cilia ultrastructure from thick sections. Proc Natl Acad Sci USA 83:9040–9044; 1986.
39. McEwen, B. F., Song, M. J., and Landis, W. J. Quantitative determination of the mineral distribution in different collagen zones of calcifying tendon using high voltage electron microscopic tomography. J Comp Assist Microsc 3:201–210; 1992.
40. Pereira, R., Khillan, J. S., Helminen, H. J., Hume, E. L., and Prockop, D. J. Transgenic mice expressing a partially deleted gene for type I procollagen (COL1A1). A breeding line with a phenotype of spontaneous fractures and decreased bone collagen and mineral. J Clin Invest 91:709–716; 1993.
41. Radermacher, M. Weighted back-projection methods. Frank, J., ed. Electron tomography. New York: Plenum Press; 1992; 91–115.
42. Radermacher, M. and Frank, J. Representation of three-dimensional reconstructed objects in electron microscopy by surfaces of equal density. J. Microsc 136:77–85; 1984.
43. Rowe, D. W., Shapiro, J. R., Poirier, M., and Schlesinger, S. Diminished type I collagen synthesis and reduced α1(I) collagen mRNA in cultured fibroblasts from patients with dominantly inherited (type I) osteogenesis imperfecta. J Clin Invest 76:604–611; 1985.
44. Sillence, D. O., Senn, A., and Danks, D. M. Genetic heterogeneity in osteogenesis imperfecta. J Med Genet 16:101–116; 1979.
45. Stacey, A., Bateman, J., Choi, T., Mascara, T., Cole, W., and Jaenisch, R.

Perinatal lethal osteogenesis imperfecta in transgenic mice bearing an engineered mutant pro α1(I) collagen gene. Nature 332:131–136; 1988.
46. Sykes, B. Bone disease cracks genetics. Nature 348:18–20; 1990.
47. Tochon-Danguy, H. J., Geoffroy, M., Boivin, G., and Baud, C. A. Mineral substance of bone tissue and of experimental cutaneous calcinosis in rats: Chemical analysis and ESR study. Calcif Tissue Int 26:259–265; 1978.
48. Torre-Blanco, A., Adachi, E., Romanic, A. M., and Prockop, D. J. Copolymerization of normal type I collagen with three mutated type I collagens containing substitutions of cysteine at different glycine positions in the α1(I) chain. J Biol Chem 267:4968–4973; 1992.
49. Traub, W., Arad, T., Vetter, U., and Weiner, S. Ultrastructural studies of bones from patients with osteogenesis imperfecta. Matrix Biol 14:337–345; 1994.
50. Traub, W., Arad, T., and Weiner, S. Three dimensional ordered distribution of crystals in turkey tendon collagen fibers. Proc Natl Acad Sci USA 86:9822–9826; 1989.
51. Vetter, U., Eanes, E. D., Kopp, J. B., Termine, J. D., and Gehron Robey, P. Changes in apatite crystal size in bones of patients with osteogenesis imperfecta. Calcif Tissue Int 49:248–250; 1991.
52. Vetter, U., Fisher, L. W., Mintz, K. P., Kopp, J. B., Tuross, N., Termine, J. D., and Gehron Robey, P. Osteogenesis imperfecta: Changes in noncollagenous proteins in bone. J Bone Min Res 6:501–505; 1991.
53. Vetter, U., Weis, M. A., Mörike, M., Eanes, E. D., and Eyre, D. R. Collagen crosslinks and mineral crystallinity in bone of patients with osteogenesis imperfecta. J Bone Min Res 8:133–137; 1993.
54. Wagner, H. D. and Weiner, S. On the relationship between the microstructure of bone and its mechanical stiffness. J Biomech 25:1311–1320; 1992.
55. Walzer, C., Boivin, G., Schönbörner, A. A., and Baud, C. A. Ultrastructural and cytochemical aspects of the initial phases of an experimental cutaneous calcinosis (calcergy) in the rat. Cell Tissue Res 212:185–202; 1980.
56. Weiner, S. and Traub, W. Crystal size and organization in bone. Connect Tissue Res 21:259–265; 1989.
57. Yamauchi, M., Katz, E. P., Otsubo, K., Teraoka, K., and Mechanic, G. L. Crosslinking and stereospecific structure of collagen in mineralized and nonmineralized skeletal tissues. Connect Tissue Res 21:159–169; 1989.

Date Received: September 6, 1994
Date Revised: January 17, 1995
Date Accepted: January 25, 1995